Selective deletion of interleukin-1 alpha in microglia regulates neuronal responses and neurorepair processes after experimental ischemic stroke.

Eloise Lemarchand[1,2] PhD[†], lemarchand@cyceron.fr, https://orcid.org/0000-0001-6781-0444; Alba Grayston[1,2] PhD[†], alba.grayston-morales@manchester.ac.uk, https://orcid.org/0000-0002-1466-0099; Raymond Wong[1,2] PhD[†], raymond.wong-2@manchester.ac.uk, https://orcid.org/0000-0003-4401-4263; Miyako Rogers[1,2], miyako.rogers@gmail.com, https://orcid.org/0009-0006-9995-8359; Blake Ouvrier[3] PhD, bouvrier@tulane.edu, https://orcid.org/0009-0006-9113-0215; Benjamin Llewellyn[1,2], benjamin.llewellyn@student.manchester.ac.uk, https://orcid.org/0009-0001-1496-0032; Freddie Webb[1,2], freddiewebb@hotmail.com, https://orcid.org/0009-0003-6703-0124; Nikolett Lénárt[4], PhD, nikolett.lenart@koki.hun-ren.hu, https://orcid.org/0000-0002-7456-949X; Adam Denes[4] PhD, denes.adam@koki.hun-ren.hu, https://orcid.org/0000-0001-6919-4905; David Brough[1,2] PhD, david.brough@manchester.ac.uk, https://orcid.org/0000-0002-2250-2381; Stuart M Allan[1,2] PhD, stuart.allan@manchester.ac.uk, https://orcid.org/0000-0001-9646-4456; Gregory Bix[3] PhD*, gbix@tulane.edu, https://orcid.org/0000-0002-8969-9553; Emmanuel Pinteaux[1,2] PhD*, emmanuel.pinteaux@manchester.ac.uk, https://orcid.org/0000-0002-9986-4401.

[1]Division of Neuroscience, School of Biological Sciences, Faculty of Biology, Medicine and Health (FBMH), The University of Manchester, Manchester, UK.

[2]Geoffrey Jefferson Brain Research Centre, University of Manchester, Northern Care Alliance NHS Foundation Trust, The Manchester Academic Health Science Centre, Manchester, UK.

[3]Department of Neurosurgery, Clinical Neuroscience Research Center, Tulane University School of Medicine, Orleans, LA, USA.

[4]"Momentum" Laboratory of Neuroimmunology, HUN-REN Institute of Experimental Medicine, Budapest, Hungary.

[†]Joint First Authors

*Joint Senior Authors

Corresponding Authors: Dr Emmanuel Pinteaux; Email: emmanuel.pinteaux@manchester.ac.uk; FBMH, University of Manchester, AV Hill Building, Manchester M13 9PT, United Kingdom. Dr Gregory Bix, Email: gbix@tulane.edu; Department of Neurosurgery, Clinical Neuroscience Research Center, Tulane University School of Medicine, New Orleans, LA, USA.

Data availability

The transcriptome dataset that supports the findings of this study are openly available at https://doi.org/10.6084/m9.figshare.25471963.v1. All other data are available upon reasonable request to the corresponding author.

Preprint statement

A preprint of this paper has been made available publicly via the preprint server BioRxiv prior to submission to submission to GLIA (doi: https://doi.org/10.1101/2024.02.16.580635). The authors hold the copyright of this preprint, with all rights reserved and no reuse allowed without permission. Upon acceptance for publication, copyright would be assigned to GLIA, and the corresponding bioRxiv entry duly linked to the DOI for the published version.

Acknowledgements

The authors would like to thank the Bioimaging Facility, the Preclinical-MRI Facility and the Genomic Technologies Facility in the FBMH at the University of Manchester for equipment and advice in imaging.

Funding

This work has been supported under the National Institute of Health (NIH, USA), National Institute of Neurological Disorders and Stroke (NINDS), R01 grant number R01NS101752 (to E.P. and G.JB.), the British Heart Foundation (BHF, UK), research grant number PG/21/10730 (to E.P., S.M.A. and D.B.), and the Leducq Foundation Transatlantic Network of Excellence: Stroke-IMPaCT 19CVD01 (to S.M.A.). D.B. is funded by Medical Research Council (MRC) grant MR/T016515/1.

Disclosures

The authors declare no conflicts of interest.

Ethics approval for the use of animals

All animal procedures were carried out in accordance with the Animals (Scientific Procedures) Act (1986), under a Home Office UK project license, approved by the local Animal Welfare Ethical Review Board, and experiments were performed in accordance with ARRIVE (Animal Research: Reporting of In Vivo Experiments) guidelines [10], with researchers blinded to experimental groups.

Abstract

Inflammation is a key contributor to stroke pathogenesis and drives exacerbated brain damage leading to poor outcome. Interleukin-1 (IL-1) is an important regulator of post-stroke inflammation, and blocking its actions is beneficial in pre-clinical stroke models and safe in the clinical setting. IL-1α and IL-1β are the two major IL-1 type 1 receptor (IL-1R1) agonists from the IL-1 family. The distinct roles of both isoforms, and particularly that of IL-1α, remain largely unknown. Here we show that IL-1α and IL-1β have different spatio-temporal expression profiles in the brain after experimental stroke, with early microglial IL-1α expression (4 h) and delayed IL-1β expression in infiltrated neutrophils and a small microglial subset (24-72 h). We examined the specific contribution of microglial-derived IL-1α in experimental permanent and transient ischemic stroke through cell-specific tamoxifen-inducible Cre-loxP-mediated recombination. Microglial IL-1α deletion did not influence acute brain damage, cerebral blood flow, IL-1β expression, neutrophil infiltration, microglial nor endothelial activation after ischemic stroke. However, microglial IL-1α knock out (KO) mice showed reduced peri-infarct vessel density and reactive astrogliosis at 14 days post-stroke, alongside a worse functional recovery. RNA sequencing analysis and subsequent pathway analysis on ipsilateral/contralateral cortex 4 h after stroke revealed a downregulation of the neuronal CREB signaling pathway in microglial IL-1α KO compared to WT mice. Our study identifies for the first time a critical role for microglial IL-1α on neuronal activity, neurorepair and functional recovery after stroke, highlighting the importance of targeting specific IL-1 mechanisms in brain injury to develop more effective therapies.

Introduction

Inflammation is a major contributor to stroke pathogenesis, and the role of inflammation driven by the pro-inflammatory cytokine interleukin-1 (IL-1) during post-stroke injury has been the focus of intense research. Indeed, pre-clinical studies have demonstrated the deleterious actions of IL-1 after stroke, whilst blocking its actions with the IL-1 receptor antagonist (IL-1Ra) is beneficial in experimental stroke [1] and safe in the clinical setting [2]. The cellular targets and actions of IL-1 in stroke are unclear, although IL-1 receptors (primarily the IL-1R1) are expressed mainly on brain endothelial cells, and we have recently demonstrated, using cell-specific conditional gene deletion of IL-1R1, that brain endothelial cells and neurons are key targets of IL-1 in stroke [3]. IL-1α and IL-1β are the two main agonists of the 11 members in the IL-1 family and they are expressed centrally and peripherally after stroke. The precise role and mechanisms of action of IL-1α remain largely unknown [4]. However, early studies suggested that IL-1α and IL-1β may exert specific differential actions during inflammation [5, 6] and, more recently, these isoforms were found to show a differential expression after experimental stroke, with early IL-1α expression in microglia preceding that of IL-1β [7]. Furthermore, our recently published work found that IL-1α, but not IL-1β, selectively triggers angiogenesis *in vitro* [8] and IL-1α given at a low dose triggers angiogenesis and improves functional recovery after stroke [9], suggesting a specific role for IL-1α distinct to that of IL-1β after stroke.

Here we show that IL-1α is expressed by microglia early after stroke, followed by a later IL-1β expression in infiltrated neutrophils and a small microglial subset. Using a genetic mouse model allowing cell-specific deletion of IL-1α, we examined the specific contribution of microglial-derived IL-1α in ischemic stroke. Selective microglial IL-1α deletion did not modify acute outcome but regulated acute neuronal activity and impaired neurorepair processes and long-term functional recovery after experimental ischemic stroke. These data reveal a potential critical role for microglial IL-1α in stroke and highlight the need for a much greater understanding of the respective contributions of IL-1 family members to cerebral ischemia, to allow the most efficient treatments to be developed.

Methods

Animals

All animal procedures were carried out in accordance with the Animals (Scientific Procedures) Act (1986), under a Home Office UK project license, approved by the local Animal Welfare Ethical Review Board, and experiments were performed in accordance with ARRIVE (Animal Research: Reporting of In Vivo Experiments) guidelines [10], with researchers blinded to genotype.

Animals were housed in groups at 21±1°C, 55±10% humidity on a 12h light-dark cycle in Sealsafe Plus Mouse individually ventilated cages (Techniplast, Italy). Mice were supplied with Sizzle Nest nesting material (Datesand Ltd., UK) and cardboard enrichment tubes (Datesand Ltd., UK), and had *ad libitum* access to standard rodent diet (SDS, UK) and water. Mice were acclimatized to the facility for at least 1 week before the commencement of experimental work.

Experiments were performed on a total of 27 C57BL/6NCrl male mice (Charles River, UK) and on a total of 88 C57BL/6J male mice from an in-house colony (IL-1α$^{fl/fl}$ and IL-1α$^{fl/fl}$:Cx3cr1^{ERT2}) at the University of Manchester. Complete schemes of the experimental designs are presented in Figures 1 to 5 and Supplementary Figures 1 to 3. A total of 18 mice were excluded: 11 due to failure/complications of the experimental procedures, 1 due to mortality after intervention and 6 culled due to declining post-stroke health issues. Experiments using the in-house colony were performed on littermate controls. Microglial specific IL-1α knockout mice were generated by mice in which exon 4 is flanked with loxP sites (IL-1α$^{fl/fl}$ [11]) with mice expressing CX3CR1 promoter-driven Cre recombinase (Cx3CR1-Cre^{ERT2}, JAX stock #020940) [12] that is expressed in the mononuclear phagocyte system. To induce CreERT2 activity and Cre-loxP-mediated deletion of IL-1α in CX3CR1-expressing cells, 3-6-month-old mice were given tamoxifen by intraperitoneal injection for 5 consecutive days (2mg/100ul in corn oil, 75 mg/kg, Sigma-Aldrich). Control mice were IL-1α$^{fl/fl}$ treated with tamoxifen. Mice were recovered for 4 weeks after tamoxifen treatment to allow the peripheral myeloid WT population to replenish, with sustained IL-1α deletion in microglia.

Focal cerebral ischemia

Two different surgical models were used to induce a permanent or transient middle cerebral artery occlusion (pMCAo and tMCAo, respectively) as models of focal ischemic stroke.

Distal $FeCl_3$-induced pMCAo was performed as a model of thrombotic cerebral ischemia, as described previously [13]. In brief, mice were anesthetized with 4% isoflurane, placed in a stereotaxic device, and maintained under anesthesia with 2% isoflurane in a 70:30% mixture of

N_2O/O_2. A small craniotomy (1 mm diameter) was performed on the parietal bone to expose the right MCA. A Whatman filter paper strip soaked in $FeCl_3$ (40%, Sigma-Aldrich) was placed on the dura mater on top of the MCA for 2 times 5 min. Cerebral blood flow (CBF) in the MCA territory was measured continuously by laser Doppler flowmetry (Oxford Optronix, UK). A total of 11 mice were excluded from the study due to clot instability leading to inadequate occlusion and absence of ischemic lesion.

Transient focal cerebral ischemia was induced for 30 min using the intraluminal filament model of proximal tMCAo as previously described [13]. Briefly, mice were anesthetized with isoflurane (4% for induction and 2% for maintenance in 30:70% mixture of N_2O/O_2, a midline incision was made on the ventral surface of the neck and the left common carotid artery isolated and ligated. A 6-0 monofilament (Doccol, Sharon, MA, USA) was introduced into the internal carotid artery via an incision in the common carotid artery. The filament was advanced approximately 10 mm into the common carotid with the filament making its way distal to the carotid bifurcation, to occlude the MCA. A 10 mm mark was made on the filament to visualize the required length to be inserted beyond the carotid bifurcation. There was an attrition of animals in the experimental groups followed up to 42 days after tMCAo, with 1 spontaneous death within the first 24 h, 4 animals culled on day 1, 1 culled at day 3 and 1 culled at day 4 relating to declining post-stroke health issues.

Body temperature was monitored and maintained at 37 ± 0.5 °C throughout both pMCAo and tMCAo procedures using a homoeothermic blanket and rectal probe (Harvard Apparatus, UK). Topical anesthetic (EMLA, 5% prilocaine and lidocaine, AstraZeneca, UK) was applied to skin incision sites prior to incision. Buprenorphine (0.05 mg/kg) was administered via subcutaneous injection at the time of surgery and at 24 h. Mice were weighed daily for the first week post-stroke, given mashed diet and administered with 0.5 ml saline daily until body weight stabilized (approximately at 4 days post-stroke).

Laser Speckle Contrast Imaging (LSCI)

At 24 h after stroke induction, a laser speckle contrast imager (moorFLPI-2, Moor Instruments, UK) was used to measure CBF. Briefly, mice were anesthetized with isoflurane (4% for induction and 2% for maintenance in 30:70% mixture of N_2O/O_2) and fixed in a stereotaxic frame with ear bars and mouth bar to prevent movement. The scalp was exposed by a mid-line skin cut, and the skin was secured away using surgical clips to clear the skull at the region for imaging. An ultrasound gel was applied to the mouse skull and a glass coverslip was mounted on top to improve image quality. The CBF was then recorded by LSCI for 3 min (20 ms exposure time, 25 frame filter). Regions of interest (ROI) were drawn on the ipsilateral and contralateral brain hemispheres and analyzed

using the moorFLPI Review V4 software (Moor Instruments) software. The % of CBF loss was calculated in the ipsilateral compared to the contralateral brain hemisphere.

Magnetic Resonance Imaging (MRI)

Mice underwent MRI scans at 4 h, 24 h and 8 days post-pMCAo. Animals were anesthetized with isoflurane (4% for induction and 2% for maintenance in 30:70% mixture of N_2O/O_2), and T2-weighted scans were conducted on Bruker Advance III console (Bruker Biospin Ltd, UK) using a 7 Tesla magnet. T2-weighted images were acquired using a multi-slice multi-echo (MSME) sequence: TE/TR 35 /7320 ms with 125 × 125 × 500 μm^3 spatial resolution. Lesion volumes were measured using ImageJ software.

Neurological deficit scoring

Mice were neurologically scored for focal deficits with the use of a 28-point neurological scoring system previously described [14]. This is a cumulative score based on the following subcategories: body symmetry, gait, climbing, circling, front limb symmetry, compulsory circling, and whisker response. Animals are ranked from 0 (normal) to 4 (extreme deficit) for each subcategory.

Tissue Processing

Anesthetized mice were transcardially perfused with cold saline followed by 50 mL of fixative (PBS 0.1 M, pH 7.4 containing 4% paraformaldehyde). Brains were removed, post-fixed (24 h), cryoprotected (sucrose 30% in PBS; 24 h), and snap-frozen in isopentane at -30˚C. Brains were then cut to a thickness of 30 µm using a freezing sledge microtome (Bright Instruments, UK) and then stored in cryoprotectant (0.05M Na2HPO4*2H2O, 5mM NaH2PO4, 30% anhydrous ethylene glycol, 20% glycerol) at -20˚C until required, for free-floating immunohistochemistry, or embedded in optimal cutting temperature compound (OCT, PFM Medical UK, Ltd) prior to snap-freezing, and cut to a thickness of 10 µm using a cryostat (Leica CM1950, UK) for on-slide immunohistochemistry.

Cresyl Violet stain

Cresyl violet staining was performed to measure lesion volume after tMCAo, as previously described [15]. Briefly, 30 µm-thick brain sections were stained with 1% cresyl violet, and cover-slipped with DPX mounting medium. For each brain, infarct volumes were measured on defined coronal sections across the whole brain, spaced at approximately 360 µm apart (using image J). Each defined coronal section, with its brain co-ordinates and lesion was integrated to estimate total lesion volume for each brain and corrected for oedema.

Immunohistochemistry

For immunostains, brain sections were washed in Dulbecco's phosphate buffeted saline (DPBS) with 0.1% Tween20, incubated in heat-mediated antigen retrieval in Tris-EDTA pH 8.6 solution for 20 min in a water bath set to 95°C, and incubated in blocking solution (1% BSA and 5% donkey serum in DPBS with 0.05% tween20, 0.1% triton X-100 and 0.2M glycine) for 1 h at room temperature. Sections were then incubated with rat–anti-Ly6G (1.25 µg/mL on-slide, 0.67 µg/mL free-floating, 127602; Biolegend), anti-Iba1 (2 µg/mL on-slide, 1 µg/mL free-floating, ab178846, Abcam), goat–anti-IL-1α (1 µg/mL, AF-400-NA; RnDSystems), goat–anti-IL-1β (1 µg/mL, AF-401-NA; RnDSystems), and glial fibrillary acidic protein (GFAP; 1:1000, Antibodies, ab4674) antibodies overnight at 4°C (in 1% BSA and 0.3% Triton X-100 in PBS). The following secondary antibodies were incubated for 2 h at room temperature: Alexa Fluor 488 donkey anti-rat, goat anti-chicken (10 µg/mL; A21208, A11039), Alexa Fluor 568 donkey anti-rabbit (10 µg/mL; A10042), and Alexa Fluor 647 donkey anti-rat, donkey anti-rabbit (10 µg/mL; A48272, A31573). IL-1β and IL-1α signal was amplified with Tyramide SuperBoostTM (Thermo Fisher) using biotinylated horse–anti-goat IgG (7.5 µg/mL, BA-9500; Vector) secondary antibody. To assess vessel density, brain slices were stained with DyLight-488 conjugated tomato lectin (1:200, ThermoFisher, L32470) during secondary antibody incubation. Sections were then washed again and counterstained with DAPI (1:20 in diluted H_2O) to stain for cell nuclei, after which they were then washed for a final time and mounted with Prolong Gold antifade reagent (Thermo Fisher Scientific; P36934).

Images were collected on Zeiss Axioimager.M2 upright microscope using a 20X Plan Apochromat objective and captured using a Coolsnap HQ2 camera (Photometrics) through Micromanager software (v1.4.23), or on a 3D-Histech Pannoramic-250 microscope slide-scanner using a x20/0.30 Plan Achromat objective (Zeiss, Germany) and captured using the Case Viewer software (3D-Histech, Hungary). Quantitative analysis was performed on 3-6 low magnification images of the lesion taken from at least 3 different coronal brain slices. Images were processed using ImageJ. Microglial activation based on morphology (Iba-1+ cells), neutrophil infiltration (Ly6G+ cells), vessel density (lectin-FITC+) and vessel activation (ICAM1+) were analyzed using the Ilastik software program [16]. To train the pixel classification algorithm, labelling was performed on at least 6 randomly selected images. All color/intensity, edge, and texture features were included, with a $\sigma 0 = 0.30$, $\sigma 1 = 0.70$, $\sigma 2 = 1.00$, $\sigma 3 = 1.60$, $\sigma 4 = 3.50$, $\sigma 5 = 5.0$ and $\sigma 6 = 10.0$.

Real-Time Quantitative Polymerase Chain Reaction

Total RNAs were extracted from samples with TRIzol Reagent (Thermo Fisher) according to the manufacturer. RNA (1 µg) was converted to cDNA using Super Script III Reverse Transcriptase (Thermo Fisher). Quantitative polymerase chain reaction (PCR) was performed using Power SYBR

Green PCR Master Mix (Thermo Fisher) in 384-well format using a 7900HT Fast Real-Time PCR System (Applied Biosystems). Three microliters of 1:20 diluted cDNA was loaded with 200 mmol/L of primers in triplicate. Data were normalized to the expression of the housekeeping gene Hmbs. Specific primers were designed using Primer3Plus software (http://www.bioinformatics.nl/cgi-bin/primer3plus/primer3plus.cgi). Primers used were: Il1b Forward—AACCTGCTGGTGTGTGACGTTC, Il1b Reverse—CAGCACGAGGCTTTTTTGTTGT, Il1a Forward—TCTCAGATTCACAACTGTTCGTG, Il1a Reverse—AGAAAATGAGGTCGGTCTCACTA. Expression levels of genes of interest were computed as follows: relative mRNA expression=$E^{-(\text{Ct of gene of interest})}$/ $E^{-(\text{Ct of housekeeping gene})}$, where Ct is the threshold cycle value and E is efficiency.

RNA-sequencing and bioinformatic analyses

Unmapped paired-end sequences from an Illumina HiSeq4000 sequencer were assessed by FastQC (http://www.bioinformatics.babraham.ac.uk/projects/fastqc/). Sequence adapters were removed, and reads were quality trimmed using Trimmomatic_0.36 [17]. The reads were mapped against the reference mouse genome (mm10) and counts per gene were calculated using annotation from GENCODE M25 (http://www.gencodegenes.org/) using STAR_2.7.2b [18]. Normalization, Principal Components Analysis, and differential expression was calculated in DESeq2_1.20.0 using default settings [19]. Canonical pathway analyses were performed using Ingenuity Pathway Analysis software (IPA, Qiagen, UK). Heatmaps were performed using MATLAB R2020a software. Venn diagrams were used to represent common and exclusive differentially expressed genes of studied groups. The exclusive genes were used independently as input for STRING protein-protein interaction (PPI) network analysis. The interactions were based on text mining, experiments, databases, co-expression, neighborhood, gene fusion and co-occurrence, considering a medium confidence (0.4) [20].

Statistical analysis

Statistical analyses were performed using GraphPad Prism 8.0. All values are expressed as mean ± standard deviation (SD) or median (InterQuartile Range, IQR) according to the normal or non-normal distribution of the represented variable, respectively. The normality of continuous variables was assessed using the Shapiro-Wilk test ($n < 30$) or Kolmogorov-Smirnov test ($n \geq 30$). Data were analyzed using unpaired t-test, one-way ANOVA (followed by Dunnet's multiple comparisons post hoc test), two-way ANOVA (followed by Dunnet's or Sidak's multiple comparisons post hoc test), or by fitting a mixed effects model using Restricted Maximum Likelihood (REML), followed by Sidak's multiple comparisons post hoc test. The Kruskal Wallis test (followed by Dunn's

multiple comparisons post hoc test) was used for non-normally distributed variables. The significant level was set at $p<0.05$.

Results

IL-1α and IL-1β are differentially expressed during the acute phase of ischemic stroke.

Gene expression of *IL1A* and *IL1B* was analyzed by RT-qPCR in the infarct, peri-infarct and contralateral brain cortical areas dissected from mice subjected to distal pMCAo at 4, 24 or 72 h post-stroke (Figure 1A). The expression of *IL1A* was affected both by time after pMCAo (p=0.0003) and amongst the dissected brain regions (p=0.0001). A significant increase of *IL1A* mRNA was observed in the peri-infarct and infarct areas at 4 h after stroke (12-fold and 28-fold increase, p=0.0116 and p=0.0001 vs. contralateral, respectively); Figure 1B. The expression of IL1B was also affected both by time after pMCAo (p=0.0339) and amongst the dissected brain regions (p=0.0007). However, IL1B mRNA expression was increased later at 24 h in the infarct areas (7-fold increase, p=0.0001 vs. contralateral); (Figure 1B). To assess the protein expression profile of IL-1 after stroke and identify the cell types expressing IL-1α and IL-1β, we performed immunostaining for both cytokines on brain sections. IL-1α was detected exclusively in microglia (Iba1+, IL-1α+), with a significantly greater expression at 4 h compared to 24 and 72 h. Specifically, 44% of microglial cells were IL-1α+ at 4 h, compared to 16% and 7% at 24 and 72 h post-MCAo, respectively (p=0.0037 and p=0.0008 vs. 24 and 72 h, respectively); (Figure 1C-D). However, IL-1β expression peaked at 24 h and was observed only in a small subset of microglia (11% at 24 h vs. 2% and 1% at 4 and 72 h post-MCAo respectively), although not reaching statistical significance between time points (p=0.0626 and p=0.9372 at 24 h vs. 4 and 72 h post-MCAo, respectively). In contrast, IL-1β was mostly expressed by neutrophils (Ly6G+), peaking at 24 h post-MCAo (29% vs. 13% at 4 and 72 h post-MCAo), again with no differences between timepoints (p=0.4815 and p=0.9999 at 24 h vs. 4 and 72 h post-MCAo, respectively. However, we did not observe significant changes between the different timepoints (p>0.05 for all comparisons; Figure 1C-D).

Successful microglial IL-1α depletion does not affect acute ischemic stroke outcome.

Based on our previous results showing that microglia are the major source of brain IL-1α acutely after stroke, we targeted microglial-derived IL-1α to investigate its specific role after stroke. Successful deletion of IL-1α in microglia was confirmed by immunohistochemistry in IL-1α$^{fl/fl}$:Cx3cr1^{ERT2} mice subjected to distal pMCAo at 4 h after stroke, which showed no IL-1α+ staining as opposed to control IL-1α$^{fl/fl}$ mice, which did show IL-1α+Iba1+ staining (Supplementary Figure 1).

First, we investigated the influence of microglial IL-1α depletion on acute stroke outcome, at 24 h after both distal pMCAo and proximal tMCAo (Figure 2).

At 24 h after pMCAo, IL-1α$^{fl/fl}$:Cx3cr1^{ERT2} mice showed no changes in lesion volume (18.2±9.9 mm^3 vs. 12.2±6.4mm^3 in the IL-1α$^{fl/fl}$ group, p=0.2060; Figure 2A-B), nor in % of CBF loss in the ipsilateral vs. contralateral brain hemisphere (-19% vs. -14% in the IL-1α$^{fl/fl}$ group, p=0.2991; Figure 2A-B). In order to assess infarct evolution beyond 24 h after pMCAo, IL-1α$^{fl/fl}$:Cx3cr1^{ERT2} mice and control IL-1α$^{fl/fl}$ mice were followed for 8 days and underwent MRI to track infarct size longitudinally at 4 h, 24 h and 8 days post-MCAo by T2-weighted imaging (T2WI), again showing no changes in lesion volume associated to genotype at the different timepoints nor in lesion volume progression with time (p>0.05 for all comparisons vs. IL-1α$^{fl/fl}$ group; Figure 3). We also investigated whether the deletion of microglial IL-1α could affect acute immune cell responses, at 24 h after pMCAo. As expected, an increase in microglial cell density was observed in the infarct areas in both IL-1α$^{fl/fl}$:Cx3cr1^{ERT2} (p=0.0069 vs. contralateral, p<0.001 vs. peri-infarct), and control IL-1α$^{fl/fl}$ mice (p=0.0069 vs. contralateral, p<0.001 vs. peri-infarct). An increase in neutrophil infiltration was also observed in the infarct areas in both IL-1α$^{fl/fl}$:Cx3cr1^{ERT2} (p=0.0357 vs. contralateral, p=0.1099 vs. peri-infarct), and control IL-1α$^{fl/fl}$ mice (p=0.0098 vs. Contralateral, p<0.001 vs. Peri-infarct). However, there were no changes between genotypes in neither microglia density nor neutrophil infiltration in the contralateral, peri-infarct and infarct areas (p>0.05 for all comparisons vs. IL-1α$^{fl/fl}$); (Supplementary Figure 2). Moreover, IL-1β expression in both microglia and neutrophils remained unchanged between genotypes (p>0.05 for all comparisons vs. IL-1α$^{fl/fl}$; Supplementary Figure 2).

At 24 h after tMCAo, IL-1α$^{fl/fl}$:Cx3cr1^{ERT2} mice showed no changes in lesion volume (46.7±15.8 mm^3 vs. 51.5±11.9 mm^3 in the IL-1α$^{fl/fl}$ group, p=0.5662; Figure 2D). The lack of effect of microglial IL-1α on brain damage was reproduced in a different tMCAo model (45 min occlusion via an incision in the external carotid artery; data not shown but available on request). We also investigated whether the deletion of microglial IL-1α could affect acute immune cell responses, at 24 h after tMCAo. No differences were observed in terms of microglial density nor activation in the contralateral, peri-infarct and infarct areas (p>0.05 for all comparisons vs. IL-1α$^{fl/fl}$). Endothelial activation, measured by the expression of ICAM-1, and neutrophil infiltration were also similar in the ipsilateral brain in both genotypes (p>0.05 for all comparisons vs. IL-1α$^{fl/fl}$); (Supplementary Figure 3).

RNA sequencing analyses revealed that microglial IL-1α is involved in CREB signaling in neurons.

Considering that microglial IL-1α expression is triggered acutely upon ischemic stroke, we aimed to further assess potential early changes in signaling pathways driven by microglial-derived IL-1α, by whole transcriptome analysis. Total RNA sequencing analysis was performed on ipsilateral and

contralateral cortex in IL-1α$^{fl/fl}$ and IL-1α$^{fl/fl}$:Cx3cr1^{ERT2} mice at 4 h after distal pMCAo, when microglial IL-1α expression peaked (Figure 4A). Details of the top 25 differentially expressed genes of each group are shown in Table 1 (ipsilateral vs. contralateral cortex, adjusted p-value < 0.05). Total RNA sequencing analysis did not reveal major changes in gene expression when comparing the respective ipsilateral nor contralateral cortex between IL-1α$^{fl/fl}$:Cx3cr1^{ERT2} and IL-1α$^{fl/fl}$ groups (Supplementary Figure 4). However, while total RNA sequencing analysis identified stroke-associated gene expression changes (ipsilateral vs. contralateral cortex), these were greatly reduced in IL-1α$^{fl/fl}$:Cx3cr1^{ERT2} mice, compared to IL-1α$^{fl/fl}$ mice. Specifically, an upregulation of 579 genes and a downregulation of 174 genes was identified in the ipsilateral cortex in IL-1α$^{fl/fl}$ mice (Figure 4B). In contrast, in IL-1α$^{fl/fl}$:Cx3cr1^{ERT2} mice we observed only 418 upregulated and 19 downregulated genes in the ipsilateral cortex (Figure 4B).

The substantial reduction in the number of up- and downregulated genes in IL-1α$^{fl/fl}$:Cx3cr1^{ERT2} mice suggests an alteration in signaling pathways upon microglial IL-1α deletion after ischemic stroke. Furthermore, amongst the top 25 differentially expressed genes for both groups (represented in Table 1), *GJB2* and *NPAS4* were found to be exclusively differentially expressed in the IL-1α$^{fl/fl}$:Cx3cr1^{ERT2} group. To further explore potential altered signaling pathways associated with microglial IL-1α expression, we sought to identify common and exclusive differentially expressed genes in the ipsilateral cortex in both groups. We found tot only 38% of all differentially expressed genes were common in both groups. In contrast, 425 genes (49%) were dysregulated exclusively in IL-1α$^{fl/fl}$ mice, while 109 genes (13%) were dysregulated exclusively in the IL-1α$^{fl/fl}$:Cx3cr1^{ERT2} group (Figure 4C). We then performed canonical pathways analysis using the IPA software. We observed that the CREB signaling in neurons pathway was the most downregulated in IL-1α$^{fl/fl}$:Cx3cr1^{ERT2} mice compared to IL-1α$^{fl/fl}$ mice, alongside other pathways such as Gαs Signaling and cAMP-mediated signaling (Figure 4D). Hierarchical clustering and heat map analysis of differentially expressed genes within the neuronal CREB signaling pathway, in ipsilateral IL-1α$^{fl/fl}$:Cx3cr1^{ERT2} and IL-1α$^{fl/fl}$ mice are represented in Figure 4E.

Effect of microglial IL-1α expression on long term outcome after ischemia reperfusion model.

We observed that animals with microglial IL-1α deletion had a worse neurological score at 14 days (9.6±2.6 vs. 6.9±1.7 in the IL-1α$^{fl/fl}$ control group, p=0.0228), at 21 days although not reaching statistical significance (8.1±1.7 vs. 4.9±2.0 in the IL-1α$^{fl/fl}$ control group, p=0.1792), and up to 28 days after tMCAo (9.2±1.7 vs. 6.4±2.6 in the IL-1α$^{fl/fl}$ control group, p=0.0229); (Figure 5B).

To explore the potential underlying mechanisms for this worse outcome, we performed histological analyses of the brains harvested at 14 days after tMCAo, when endogenous post-stroke neurorepair processes such as angiogenesis and neurogenesis are highly active [21].

Cortical peri-infarct vessel density was unchanged between ipsilateral and contralateral brain hemispheres in both groups (data not shown), whilst peri-infarct subcortical vessel density was enhanced in both IL-1α$^{fl/fl}$ and IL-1α$^{fl/fl}$:Cx3cr1^{ERT2} mice by 1.6-fold (p=0.0008 vs. contralateral) and by 1.4-fold (p=0.0269 vs. contralateral), respectively (Figure 5C), which is in line with the ischemic lesion primarily affecting subcortical areas in this model (Figure 2D). Furthermore, we observed that IL-1α$^{fl/fl}$:Cx3cr1^{ERT2} mice had a 4.9-fold decrease in the peri-infarct subcortical vessel density compared to that of IL-1α$^{fl/fl}$ (p=0.0025; Figure 5C). Along with a decreased vessel density at 14 days post-stroke, mice with microglial IL-1α depletion showed a reduced density of reactive astrocytes, measured by the GFAP+ area in the subcortical peri-infarct area (p=0.0085 vs. IL-1α$^{fl/fl}$ mice; Figure 5D).

Overall, microglial IL-1α deletion led to reduced vascular density and astrogliosis, which are known to contribute to post-stroke recovery and could therefore explain the long-term functional impairment amongst IL-1α$^{fl/fl}$:Cx3cr1^{ERT2} mice, suggesting a possible role of microglial IL-1α in post-stroke neurorepair processes.

Discussion

In this study, we show that IL-1α and IL-1β have differential spatio-temporal expression profiles in the brain after stroke, confirming earlier observations [7] and suggesting that they might exert distinct non-overlapping roles at different stages of post-stroke inflammation. Here, we show that IL-1α is expressed exclusively by microglial cells early after stroke onset, followed by a delayed IL-1β expression by a small subset of microglia and mostly by infiltrating neutrophils. Upon stroke onset, microglia are the first resident immune responders, rapidly migrating and becoming activated at the lesion site, exacerbating tissue injury by releasing pro-inflammatory cytokines and cytotoxic factors, but also contributing to tissue repair and remodeling by engulfing cellular debris and invading neutrophils, and releasing anti-inflammatory cytokines and growth factors [22, 23]. With microglia being the major source of brain IL-1α expression and considering its pivotal role in post-stroke neuroinflammation, we aimed to study the specific role of microglial IL-1α in ischemic stroke using a novel microglial-specific IL-1α deficient mouse.

Successful microglial IL-1α deletion did not influence acute brain damage and cerebral blood flow, nor infarct lesion progression as seen by MRI up to 8 days post-stroke, suggesting that microglial IL-1α might not contribute to acute brain damage, despite its very early expression. On the other hand, the effect of microglial-derived IL-1α on microglial function in stroke is completely unknown. Nonetheless, microglial proliferation is known to be the main source of microgliosis after ischemic stroke [24] and, in this regard, *IL1R1* and *IL1A* have been identified as key genes involved in microglial replenishment upon ablation in adult mice [25], while CX3CR1 has been implicated in microglial chemotaxis, microglia-mediated neurotoxicity, and microglial activation [26]. With all this in mind, we investigated whether CX3CR1-Cre-mediated microglial IL-1α deletion could affect microglial functions, such as microgliosis and neutrophil engulfment, after both transient and permanent cerebral ischemia. Microglial IL-1α ablation did not modify microglial density nor activation, neutrophil infiltration, endothelial activation, nor IL-1β expression in the brain after stroke. These results suggest that microglial IL-1α may not be involved in microglial functions nor IL-1β expression early after stroke, although future studies should include additional timepoints to elucidate potential microglial IL-1α effects on microglia in the subacute and chronic phases.

Considering that acute microglial IL-1α expression is triggered acutely upon ischemic stroke, we wanted to investigate potential early changes in signaling pathways driven by microglial-derived IL-1α. Whole RNA sequencing analysis in the brain cortex at 4 h after distal pMCAo showed striking differences in the number of downregulated and upregulated genes between microglial-IL-1α deficient and control mice. Only 38% of all differentially expressed genes were common between

IL-1α$^{fl/fl}$ and IL-1α$^{fl/fl}$:Cx3cr1^{ERT2} mice, while 109 genes were dysregulated exclusively in the IL-1α$^{fl/fl}$:Cx3cr1^{ERT2} group, 2 of which were amongst the top 25 differentially expressed genes in this group, *GJB2* and *NPAS4*. *GJB2* encodes for a gap junction protein known as Connexin 26, present in astrocytes and leptomeningial cells in the brain [27]. *NPAS4* encodes for a transcription factor whose expression is induced in upon cerebral ischemia, which has been associated with a neuroprotective role, potentially through modulation of cell death and inflammatory responses [28]. Importantly, canonical pathways analysis identified the neuronal CREB signaling pathway as the most down-regulated in the absence of microglial IL-1α expression. Our previous studies *in vitro* demonstrated that IL-1 can act on neurons to induce neuronal activation and expression of neuronal inflammatory mediators through a CREB-dependent signaling mechanism [29]. Also, CREB activity controls cortical circuit plasticity and functional recovery after stroke [30]. This is of importance since microglial IL-1α expression is associated with areas of neuronal loss in the penumbra [7], whilst complete depletion of microglia is detrimental after stroke [31, 32]. Importantly, conditional IL-1R1 deletion in neurons using tamoxifen inducible nestin-Cre mice resulted in altered microglia-neuron interaction [3]. These observations suggest that microglia IL-1α could play an important regulatory role in the neuronal response to ischemic stress. However, we were unable to identify major gene expression changes in the ipsilateral hemisphere associated with microglial IL-1α deletion in a permanent model of cerebral ischemia, at this specific timepoint and cortical brain region.

Surprisingly, despite the early expression of microglial IL-1α, which does not seem to have major effects on acute stroke outcome, its deletion was associated with a worse functional recovery from 14 days and up to 28 days after cerebral ischemia. We also observed that microglial IL-1α deficient mice had a reduced peri-infarct vessel density, suggestive of impaired post-stroke angiogenesis. Peri-infarct vascular remodeling occurs mostly during the first 2 weeks post-stroke in rodent models and is known to contribute to functional recovery [21, 33]. These results could explain the behavioral deficits in microglial IL-1α deficient mice and are in line with previous findings showing that subacute IL-1α administration increases post-stroke angiogenesis in mice [9]. Furthermore, impaired angiogenesis occurred along with reduced astrogliosis as seen by a decreased GFAP expression and a slightly lower glial scar thickness. Microglia comprise a highly heterogeneous and plastic cell population, displaying numerous overlapping functional states and participating in a complex crosstalk with different cell types within the neurovascular unit and infiltrating peripheral leukocytes [22]. In this context, microglia, which respond earlier to injury, can modulate astrocyte activation and functions. Recently, Huang et al. proposed that microglia may inhibit the recruitment of neutrophils and secondary occlusions through the release of IL-1RA, which in turn modulates

astrocytic CXCL1 expression [31]. In line with our results, a recent study showed that activated microglia induce reactive astrocytes through the release of IL-1α, TNFα, and C1q; however, this was associated with the activation of neurotoxic reactive astrocytes [34]. Interestingly, amongst the top 25 differentially expressed genes in the transcriptomic analysis at 4 h after distal pMCAo, only *NPAS4* and *GJB2*, the latter encoding for a Connexin 26, which is present in astrocytes and leptomeningial cells, were exclusively differentially expressed in the microglial IL-1α KO group. These results point towards possible early transcriptomic changes associated with microglial IL-1α that could modulate astrocyte functions and influence processes taking place later, such as angiogenesis. The role of reactive astrocytes in stroke is a subject of debate, with evidence suggesting they can both hinder and promote stroke recovery. In accordance with our results, Williamson and colleagues showed that reactive astrocytes facilitate vascular repair and remodeling, improving motor recovery after stroke [35]. However, late transcriptomic changes were not assessed in this study, and more exhaustive and integrative omics studies are warranted to gain a better understanding of the downstream effects of stroke-induced microglial IL-1α expression.

Taken together, this study identifies a critical role for microglial IL-1α in stroke, supporting that IL-1α plays a fundamentally different role to that of IL-1β in the context of stroke, and should be therefore considered as a potential therapeutic target. Our findings suggest that microglial-derived IL-1α does not modify acute stroke outcome, despite its hyperacute expression, yet it might regulate long-term cerebrovascular responses modulating functional recovery after experimental stroke. Nonetheless, the mechanisms underlying the non-redundancy of IL-1α and IL-1β, the role of microglia and the potential link with other cell types are not fully understood. Future studies focusing on the specific role of IL-1α and other IL-1 family members in stroke are needed to advance the understanding of stroke pathophysiology, which is essential to refine IL-1 targeted stroke interventions.

References

1. Mulcahy NJ, Ross J, Rothwell NJ, Loddick SA. Delayed administration of interleukin-1 receptor antagonist protects against transient cerebral ischaemia in the rat. Br J Pharmacol. 2003 Oct;140(3):471-6.
2. Smith CJ, Hulme S, Vail A, Heal C, Parry-Jones AR, Scarth S, Hopkins K, Hoadley M, Allan SM, Rothwell NJ, Hopkins SJ, Tyrrell PJ. SCIL-STROKE (Subcutaneous Interleukin-1 Receptor Antagonist in Ischemic Stroke): A Randomized Controlled Phase 2 Trial. Stroke. 2018 May;49(5):1210-1216.
3. Wong R, Lénárt N, Hill L, Toms L, Coutts G, Martinecz B, Császár E, Nyiri G, Papaemmanouil A, Waisman A, Müller W, Schwaninger M, Rothwell N, Francis S, Pinteaux E, Denés A, Allan SM. Interleukin-1 mediates ischaemic brain injury via distinct actions on endothelial cells and cholinergic neurons. Brain Behav Immun. 2019 Feb;76:126-138.
4. Sobowale OA, Parry-Jones AR, Smith CJ, Tyrrell PJ, Rothwell NJ, Allan SM. Interleukin-1 in Stroke: From Bench to Bedside. Stroke. 2016 Aug;47(8):2160-7.
5. Anforth HR, Bluthe RM, Bristow A, Hopkins S, Lenczowski MJ, Luheshi G, Lundkvist J, Michaud B, Mistry Y, Van Dam AM, Zhen C, Dantzer R, Poole S, Rothwell NJ, Tilders FJ, Wollman EE. Biological activity and brain actions of recombinant rat interleukin-1alpha and interleukin-1beta. Eur Cytokine Netw. 1998 Sep;9(3):279-88.
6. Tsakiri N, Kimber I, Rothwell NJ, Pinteaux E. Differential effects of interleukin-1 alpha and beta on interleukin-6 and chemokine synthesis in neurones. Mol Cell Neurosci. 2008 Jun;38(2):259-65.
7. Luheshi NM, Kovács KJ, Lopez-Castejon G, Brough D, Denes A. Interleukin-1α expression precedes IL-1β after ischemic brain injury and is localised to areas of focal neuronal loss and penumbral tissues. J Neuroinflammation. 2011 Dec 29;8:186.
8. Salmeron K, Aihara T, Redondo-Castro E, Pinteaux E, Bix G. IL-1alpha induces angiogenesis in brain endothelial cells in vitro: implications for brain angiogenesis after acute injury. J Neurochem. 2016 Feb;136(3):573-80.
9. Salmeron KE, Maniskas ME, Edwards DN, Wong R, Rajkovic I, Trout A, Rahman AA, Hamilton S, Fraser JF, Pinteaux E, Bix GJ. Interleukin 1 alpha administration is neuroprotective and neuro-restorative following experimental ischemic stroke. J Neuroinflammation. 2019 Nov 14;16(1):222.
10. Percie du Sert N, Hurst V, Ahluwalia A, Alam S, Avey MT, Baker M, et al. The ARRIVE guidelines 2.0: Updated guidelines for reporting animal research. J Cereb Blood Flow Metab. 2020;40(9):1769-77.

11. Bageghni SA, Hemmings KE, Yuldasheva NY, Maqbool A, Gamboa-Esteves FO, Humphreys NE, Jackson MS, Denton CP, Francis S, Porter KE, Ainscough JF, Pinteaux E, Drinkhill MJ, Turner NA. Fibroblast-specific deletion of interleukin-1 receptor-1 reduces adverse cardiac remodeling following myocardial infarction. JCI Insight. 2019 Aug 8;5(17):e125074.
12. Yona S, Kim KW, Wolf Y, Mildner A, Varol D, Breker M, Strauss-Ayali D, Viukov S, Guilliams M, Misharin A, Hume DA, Perlman H, Malissen B, Zelzer E, Jung S. Fate mapping reveals origins and dynamics of monocytes and tissue macrophages under homeostasis. Immunity. 2013 Jan 24;38(1):79-91.
13. Denorme F, Langhauser F, Desender L, et al. ADAMTS13-mediated thrombolysis of t-PA-resistant occlusions in ischemic stroke in mice. Blood. 2016;127(19):2337-2345.
14. Clark W, Gunion-Rinker L, Lessov N, et al. Citicoline treatment for experimental intracerebral hemorrhage in mice. Stroke 1998; 29: 2136–2140.
15. McColl BW, Rothwell NJ, Allan SM. Systemic inflammatory stimulus potentiates the acute phase and CXC chemokine responses to experimental stroke and exacerbates brain damage via interleukin-1- and neutrophil-dependent mechanisms. J Neurosci. 2007 Apr 18;27(16):4403-12.
16. Berg S, Kutra D, Kroeger T, Straehle CN, Kausler BX, Haubold C, Schiegg M, Ales J, Beier T, Rudy M, Eren K, Cervantes JI, Xu B, Beuttenmueller F, Wolny A, Zhang C, Koethe U, Hamprecht FA, Kreshuk A. ilastik: interactive machine learning for (bio)image analysis. Nat Methods. 2019 Dec;16(12):1226-1232.
17. Bolger AM, Lohse M, Usadel B. Trimmomatic: a flexible trimmer for Illumina sequence data. Bioinformatics. 2014 Aug 1;30(15):2114-20.
18. Dobin A, Davis CA, Schlesinger F, Drenkow J, Zaleski C, Jha S, Batut P, Chaisson M, Gingeras TR. STAR: ultrafast universal RNA-seq aligner. Bioinformatics. 2013 Jan 1;29(1):15-21.
19. Love MI, Huber W, Anders S. Moderated estimation of fold change and dispersion for RNA-seq data with DESeq2. Genome Biol. 2014;15(12):550.
20. Szklarczyk D, Gable AL, Nastou KC, Lyon D, Kirsch R, Pyysalo S, et al. The STRING database in 2021: customizable protein-protein networks, and functional characterization of user-uploaded gene/measurement sets. Nucleic Acids Res. 2021.
21. Williamson MR, Franzen RL, Fuertes CJA, Dunn AK, Drew MR, Jones TA. A Window of Vascular Plasticity Coupled to Behavioral Recovery after Stroke. J Neurosci. 2020 Sep 30;40(40):7651-7667.
22. Qin C, Zhou LQ, Ma XT, Hu ZW, Yang S, Chen M, Bosco DB, Wu LJ, Tian DS. Dual Functions of Microglia in Ischemic Stroke. Neurosci Bull. 2019 Oct;35(5):921-933.

23. Planas AM. Role of microglia in stroke. Glia. 2024 Jan 4. doi: 10.1002/glia.24501. Epub ahead of print. PMID: 38173414.
24. Li T, Pang S, Yu Y, Wu X, Guo J, Zhang S. Proliferation of parenchymal microglia is the main source of microgliosis after ischaemic stroke. Brain. 2013 Dec;136(Pt 12):3578-88.
25. Bruttger J, Karram K, Wörtge S, Regen T, Marini F, Hoppmann N, Klein M, Blank T, Yona S, Wolf Y, Mack M, Pinteaux E, Müller W, Zipp F, Binder H, Bopp T, Prinz M, Jung S, Waisman A. Genetic Cell Ablation Reveals Clusters of Local Self-Renewing Microglia in the Mammalian Central Nervous System. Immunity. 2015 Jul 21;43(1):92-106.
26. Liang KJ, Lee JE, Wang YD, Ma W, Fontainhas AM, Fariss RN, et al. Regulation of dynamic behavior of retinal microglia by CX3CR88 signaling. Invest Ophthalmol Vis Sci. 2009;50:4444–4451.
27. Garcia-Vega L, O'Shaughnessy EM, Albuloushi A, Martin PE. Connexins and the Epithelial Tissue Barrier: A Focus on Connexin 26. Biology (Basel). 2021 Jan 14;10(1):59.
28. Ramiro L, Faura J, Simats A, García-Rodríguez P, Ma F, Martín L, Canals F, Rosell A, Montaner J. Influence of sex, age and diabetes on brain transcriptome and proteome modifications following cerebral ischemia. BMC Neurosci. 2023 Jan 27;24(1):7.
29. Tsakiri N, Kimber I, Rothwell NJ, Pinteaux E. Mechanisms of interleukin-6 synthesis and release induced by interleukin-1 and cell depolarisation in neurones. Mol Cell Neurosci. 2008 Jan;37(1):110-8.
30. Caracciolo L, Marosi M, Mazzitelli J, Latifi S, Sano Y, Galvan L, Kawaguchi R, Holley S, Levine MS, Coppola G, Portera-Cailliau C, Silva AJ, Carmichael ST. CREB controls cortical circuit plasticity and functional recovery after stroke. Nat Commun. 2018 Jun 8;9(1):2250. doi: 10.1038/s41467-018-04445-9. PMID: 29884780; PMCID: PMC5993731.
31. Krupinski J, Kaluza J, Kumar P, et al. Role of angiogenesis in patients with cerebral ischemic stroke. Stroke 1994; 25: 1794–1798.
32. Lalancette-Hébert M, Gowing G, Simard A, Weng YC, Kriz J. Selective ablation of proliferating microglial cells exacerbates ischemic injury in the brain. J Neurosci. 2007 Mar 7;27(10):2596-605.
33. Huang X, Guo M, Zhang Y, Xie J, Huang R, Zuo Z, Saw PE, Cao M. Microglial IL-1RA ameliorates brain injury after ischemic stroke by inhibiting astrocytic CXCL1-mediated neutrophil recruitment and microvessel occlusion. Glia. 2023 Jul;71(7):1607-1625.
34. Liddelow SA, Guttenplan KA, Clarke LE, Bennett FC, Bohlen CJ, Schirmer L, Bennett ML, Münch AE, Chung WS, Peterson TC, Wilton DK, Frouin A, Napier BA, Panicker N, Kumar M, Buckwalter MS, Rowitch DH, Dawson VL, Dawson TM, Stevens B, Barres BA. Neurotoxic

reactive astrocytes are induced by activated microglia. Nature. 2017 Jan 26;541(7638):481-487.

35. Williamson MR, Fuertes CJA, Dunn AK, Drew MR, Jones TA. Reactive astrocytes facilitate vascular repair and remodeling after stroke. Cell Rep. 2021 Apr 27;35(4):109048.

Tables

Table 1. Top 25 differentially expressed genes between the infarcted ipsilateral hemisphere and the contralateral healthy hemisphere 4 h after pMCAo. Genes that are differentially expressed exclusively in one of the groups are highlighted in bold. Log2FC: binary logarithm of the fold change.

IL-1α$^{fl/fl}$			**IL-1α$^{fl/fl}$:Cx3cr1^{ERT2}**		
Gene symbol	**Log2FC**	**Adj. p-value**	**Gene symbol**	**Log2FC**	**Adj. p-value**
ATF3	3.620	4.35E-36	***GJB2***	**2.374**	**1.47E-36**
AKAP12	1.342	3.87E-31	*AKAP12*	1.391	1.21E-31
ADAMTS1	1.578	2.54E-25	*HSPA1B*	4.415	4.16E-27
BCOR	1.044	4.13E-23	*ATF3*	3.647	4.12E-25
CD14	2.499	9.91E-21	*ADAMTS1*	1.770	4.12E-25
ZBTB1	1.276	1.21E-20	*CD14*	3.015	3.97E-23
GADD45B	1.491	3.09E-20	*A2M*	2.577	4.99E-22
RIMBP2	0.632	2.72E-17	*FOS*	1.297	1.31E-21
SOCS3	2.001	1.49E-16	*JUN*	1.244	2.45E-21
PTGS2	1.048	2.91E-16	*HSPA1A*	4.129	1.05E-20
MIR670HG	2.140	4.99E-16	*CCL3*	5.430	3.26E-19
CCL3	4.766	3.62E-15	***NPAS4***	**1.282**	**8.48E-18**
RGS2	1.027	5.57E-15	*SOCS3*	2.018	1.67E-17
SERTAD1	1.418	9.78E-15	*MIR670HG*	2.122	1.45E-15
GRASP	0.782	9.78E-15	*HMOX1*	1.681	2.62E-14
LRRC32	1.813	6.93E-14	*PTGS2*	1.117	3.68E-14
IGSF9	1.833	7.16E-14	*HSPH1*	0.787	3.68E-14
GDPD5	0.911	7.33E-14	*TRIP10*	1.592	5.15E-14
PPM1H	0.728	1.02E-13	*RGS2*	1.117	2.29E-13
FAM126B	0.581	2.73E-12	*BCOR*	1.139	4.43E-13
HSPA5	0.561	7.15E-12	*GADD45B*	1.384	1.62E-12
EFCAB6	1.299	2.07E-11	*ZBTB1*	1.288	3.88E-12
GLCE	0.856	2.38E-11	*DNAJB1*	0.995	7.66E-12
TMEM252	1.544	2.69E-11	*PPM1H*	0.851	9.81E-12
SEMA4A	0.694	4.35E-11	*IGSF9*	1.690	1.54E-11

Figures

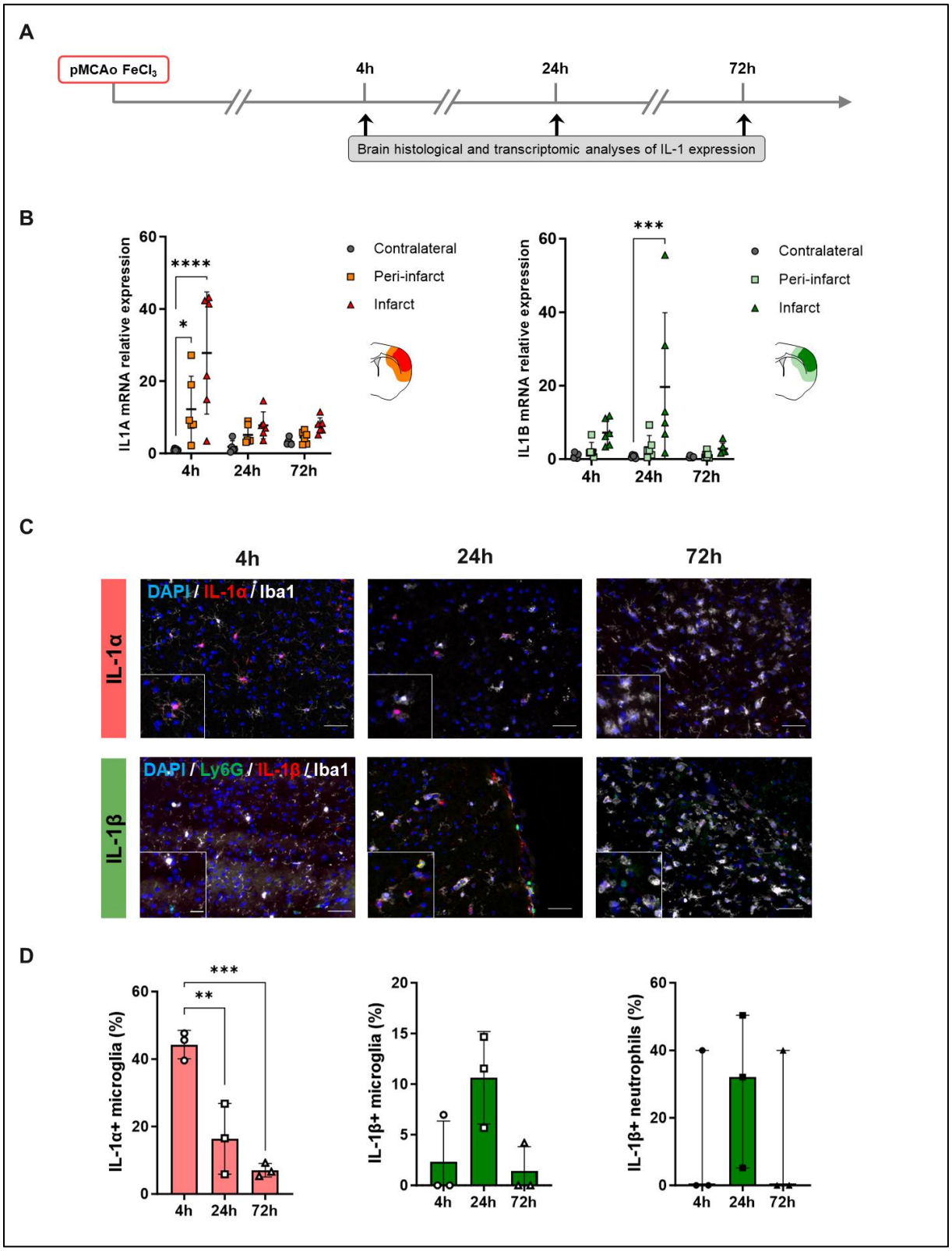

Figure 1. IL-1 brain expression during the early phase of distal pMCAo. (A) Schematic representation of the experimental design. (B) RT-qPCR analysis showing different spatio-temporal

expression of *IL1A* (left) and IL1B (right) in the contralateral, peri-infarct and infarct areas at 4, 24 and 72 h after stroke (mRNA levels normalized to contralateral at 4 h); n=6/group, *p<0.05, ****p<0.0001 vs. contralateral, two-way ANOVA followed by Dunnet's post hoc test. (C) Representative immunostaining of IL-1α (red), microglia (Iba1, white), neutrophils (Ly6G, green), IL-1β (red), and DAPI (blue) in the infarct at 4, 24 and 72 h after stroke. Scale bar in the large image is 50 μm and in the inset is 20 μm. (D) Percentage of IL-1α positive microglia in the infarct at 4, 24 and 72 h after stroke. (left; n=3/group, ***p<0.001, one-way ANOVA followed by Dunnet's post hoc test). Percentage of IL-1β positive microglia and IL-1β positive neutrophils in the contralateral, peri-infarct and infarct areas at 4, 24 and 72 h after stroke. (right; n=3/group, one-way ANOVA or Kruskal-Wallis followed by Dunnet's or Dunn's post hoc test).

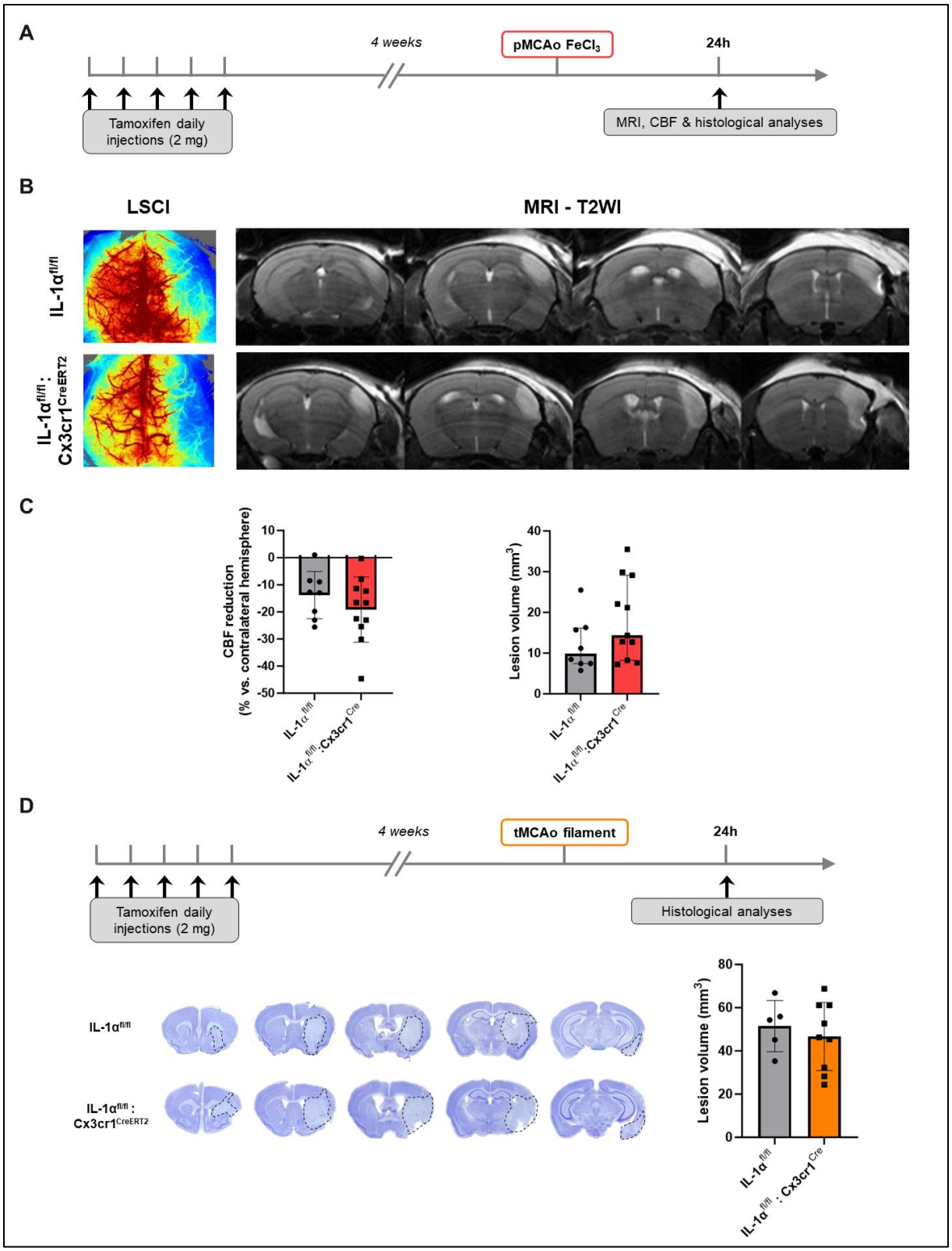

Figure 2. Microglial IL-1α deletion does not influence brain damage or cerebral blood flow at 24 hours after permanent nor transient cerebral ischemia. (A) Schematic representation of the experimental design to study acute outcome after permanent stroke. (B) Representative LSCI and CBF reduction quantification (left) and representative T2-WI and lesion volume quantification

(right) at 24 h after pMCAo in IL-1α$^{fl/fl}$ and IL-1α$^{fl/fl}$:Cx3cr1^{ERT2} mice (n=8-11/group, unpaired t-test). (C) Schematic representation of the experimental design to study acute outcome after transient stroke. (D) Representative cresyl violet-stained brains (lesion delineated by dashed lines) and lesion volume quantification (n=5-9/group, unpaired t-test).

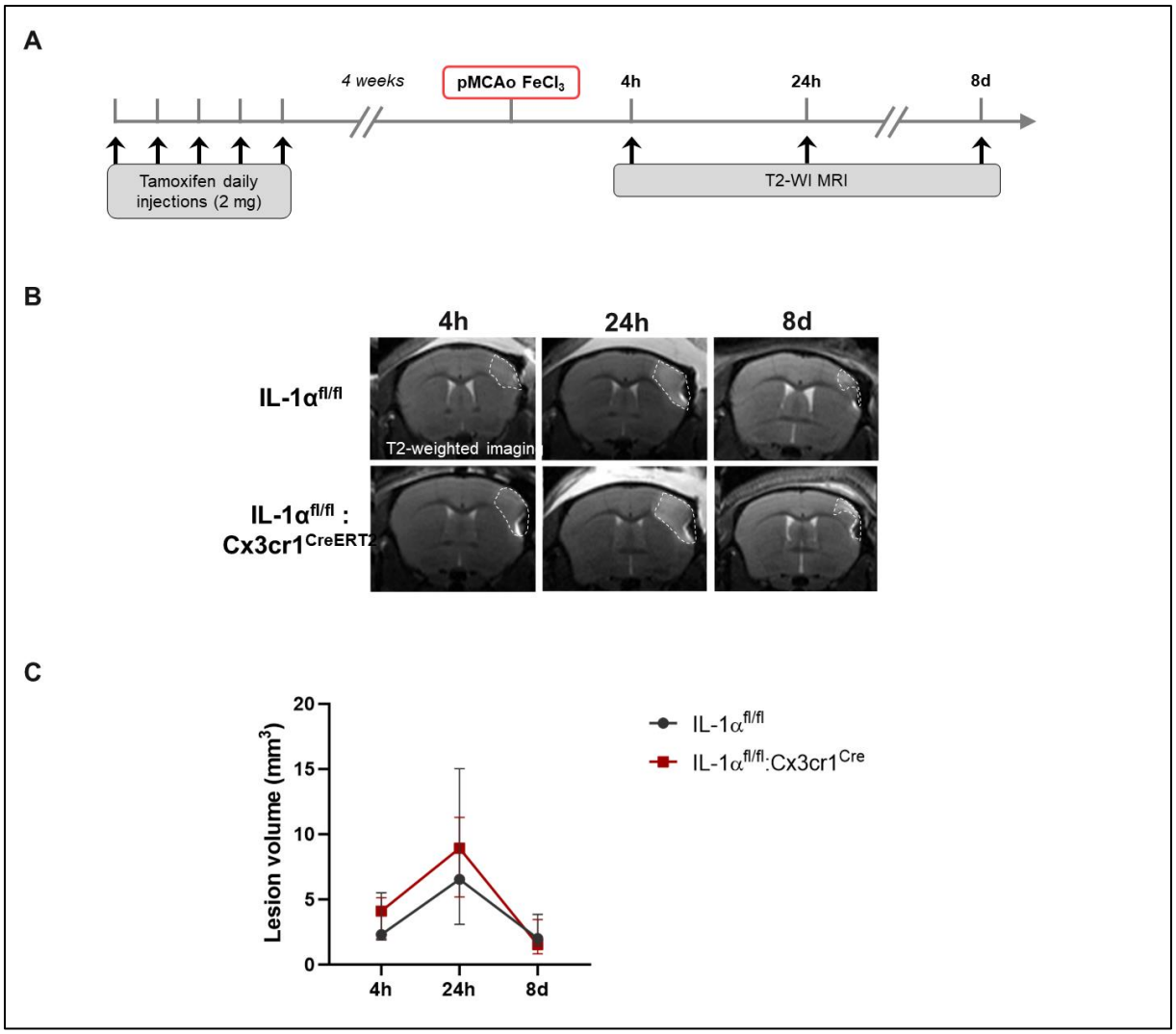

Figure 3. Microglial IL-1α deletion does not influence brain lesion progression up to 8 days after permanent cerebral ischemia. (A) Schematic representation of the experimental design. (B) Representative T2-WI at 4 h, 24 h and 8 days after pMCAo. (C) Lesion volume quantification showing no differences between IL-1α$^{fl/fl}$ and IL-1α$^{fl/fl}$:Cx3cr1^{ERT2} mice (n=4/group, two-way ANOVA followed by Sidak's post hoc test).

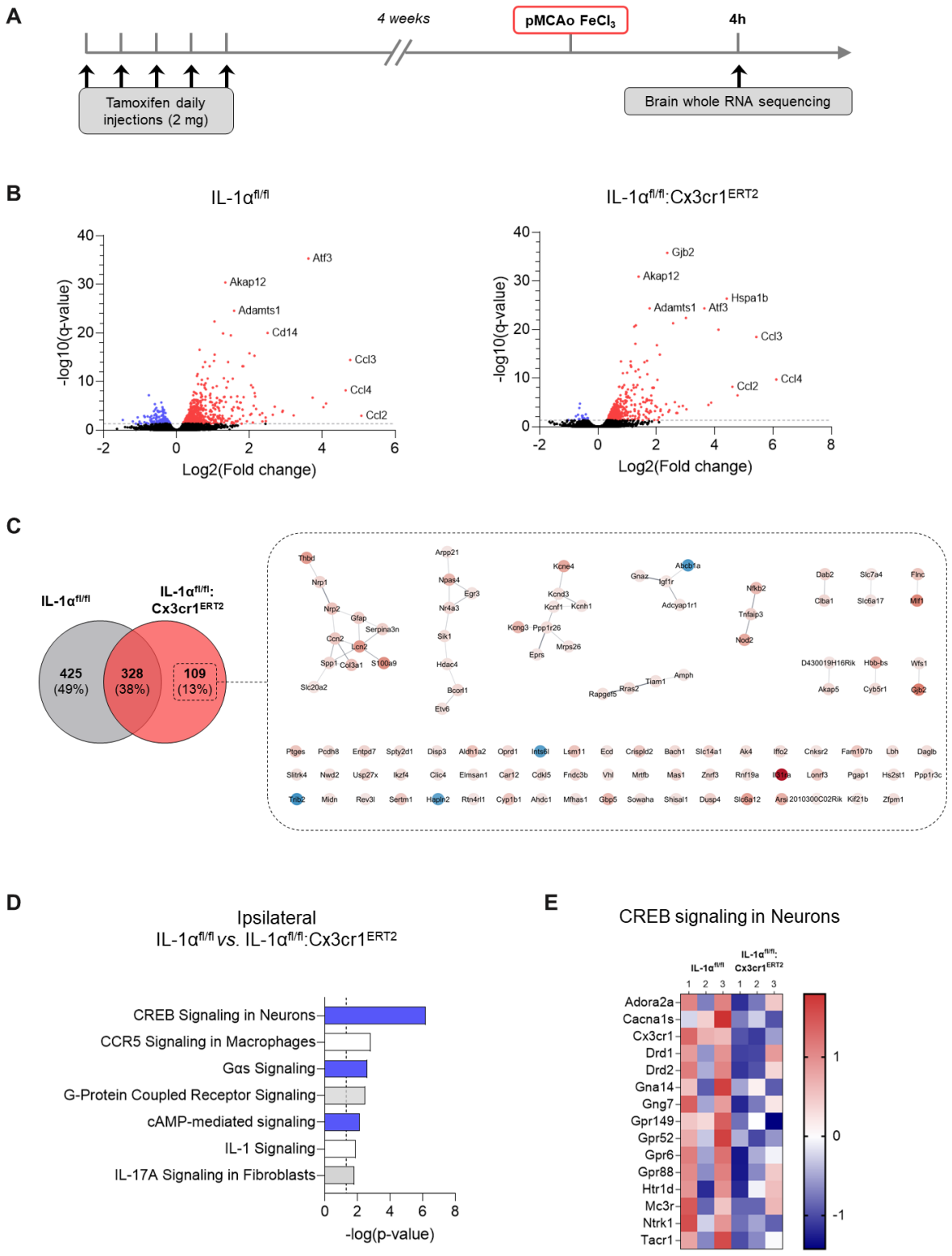

Figure 4. RNA sequencing analysis performed 4h after permanent cerebral ischemia revealed that microglial IL-1α could regulate neuronal activity through CREB signaling. (A) Schematic representation of the experimental design. (B) Volcano plot showing genes upregulated (red) and downregulated (blue) in the ipsilateral cortex 4 h after distal pMCAo in IL-1α$^{fl/fl}$ mice (left),

and showing genes upregulated (red) and downregulated (blue) in the ipsilateral cortex 4 h after pMCAo in IL-1α$^{fl/fl}$:Cx3cr1^{ERT2} mice (right). (C) Venn diagram of differentially expressed genes in the ischemic cortex in both groups. The 109 exclusively differentially expressed genes in IL-1α$^{fl/fl}$:Cx3cr1^{ERT2} mice are shown through a STRING network revealing the main interactions between molecules. The strength of the correlation between two genes (nodes) is reflected by the thickness of the edge, and color mapping based on the log2FC values (red indicating higher log2FC and blue indicating lower log2FC). (D) Bar graph showing canonical pathway changes in ipsilateral IL-1α$^{fl/fl}$:Cx3cr1^{ERT2} vs. IL-1α$^{fl/fl}$ mice (blue: negative z-score, white: z-score = 0, grey: no activity pattern available). (E) Hierarchical clustering and heat map analysis of differentially expressed genes (15 genes) within the neuronal CREB signaling pathway, in ipsilateral IL-1α$^{fl/fl}$:Cx3cr1^{ERT2} and IL-1α$^{fl/fl}$ mice. The scaled expression value (row z-score) is shown in a blue-red color scheme, red indicating higher expression and blue indicating lower expression (n=3/group).

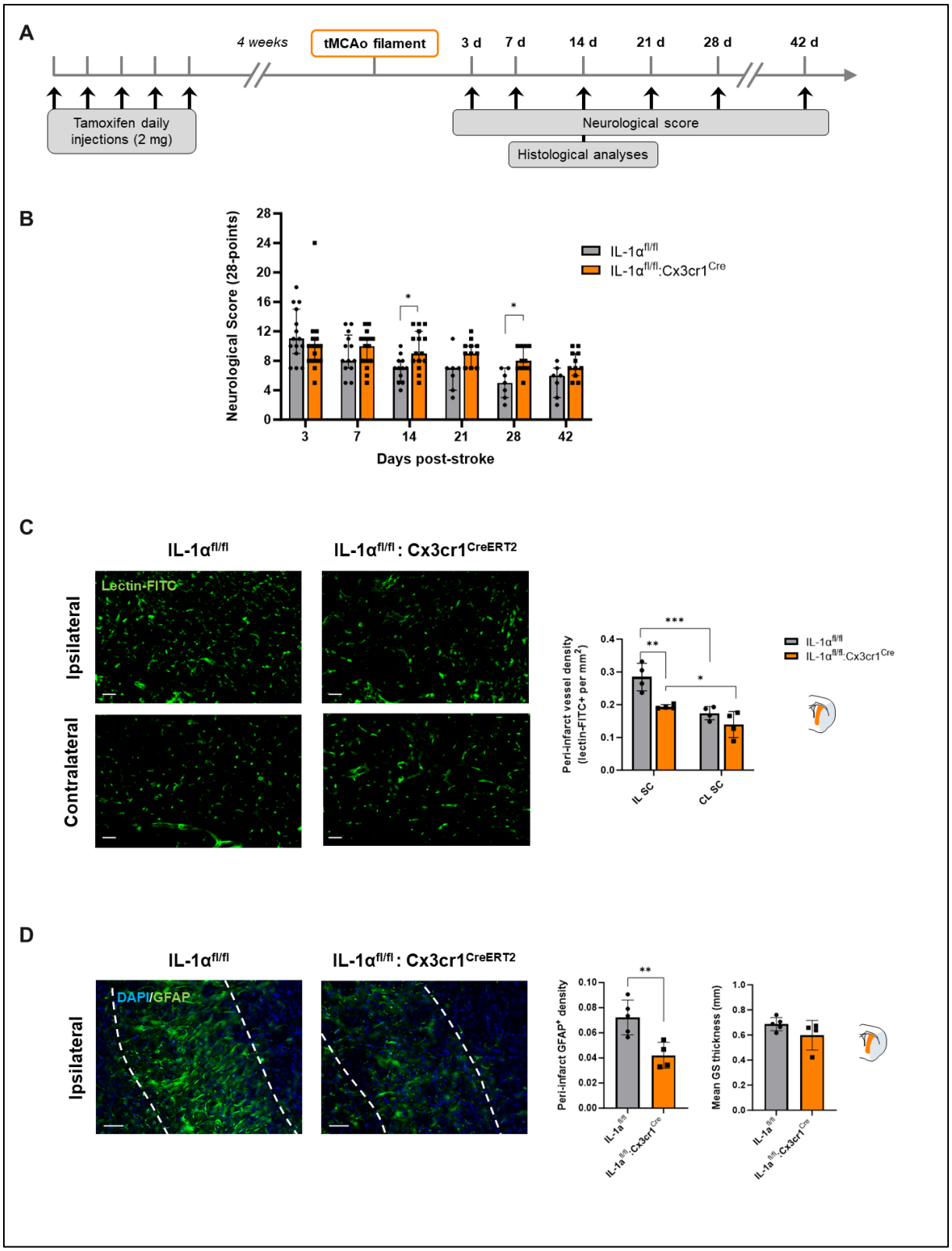

Figure 5. Effect of microglial IL-1α deletion on long-term stroke outcome. (A) Schematic representation of the experimental design. (B) 28-point neurological score showing significant functional deficit IL-1α$^{fl/fl}$:Cx3cr1^{ERT2} compared to in IL-1α$^{fl/fl}$ mice, 14 and 28 days after tMCAo (n=15-16, *p<0.05 mixed effects model (REML) followed by Sidak's post hoc test). (C) Representative

immunostaining of vascular density (lectin-FITC+) in the ipsilateral peri-infarct and corresponding contralateral subcortical brain regions in IL-1α$^{fl/fl}$ and IL-1α$^{fl/fl}$:Cx3cr1^{ERT2} mice, and quantification (Scale bar: 50 µm, n=4/group, two-way ANOVA followed by Sidak's post hoc test). (D) Representative immunostaining of the glial scar (GFAP+) in the ipsilateral peri-infarct subcortical brain region in IL-1α$^{fl/fl}$ and IL-1α$^{fl/fl}$:Cx3cr1^{ERT2} mice, and quantification of the GFAP+ density (left) and glial scar (GS) thickness (right) (Scale bar: 50 µm, n=4-5/group, unpaired t-test, **$p<0.01$).